



Search for New Heavy Charged Gauge Bosons

Decaying in the Electron Channel

The DØ Collaboration
URL <http://www-d0.fnal.gov>

Additional gauge bosons are introduced in many theoretical extensions to the standard model. This note describes the search for a new heavy charged gauge boson W' decaying into an electron and a neutrino. The data used in this analysis was taken with the DØ Detector at the Fermilab Tevatron $p\bar{p}$ collider at a center-of-mass energy of 1.96 TeV and corresponds to an integrated luminosity of 900 pb^{-1} . Since we do not see any significant excess in the data, an upper limit is set on the production cross section times branching ratio $\sigma_{W'} \times B(W' \rightarrow e\nu)$. Using this limit, a W' boson with mass below 965 GeV can be excluded at the 95% confidence level assuming that the new boson has the same couplings to fermions as the standard model W boson.

Preliminary Results for Summer 2006 Conferences

The standard model (SM) describes the fundamental fermions and their interactions via gauge bosons in a reasonable way, but it is not considered to be a complete theory. Some aspects – like the number of fermion families and the hierarchy of fermion masses – remain unexplained. There are many possible extensions to the SM, where some of them introduce an additional charged gauge boson W' [1].

Additional gauge bosons (including the equivalent to the Z , the Z') are introduced in e.g. Left-Right-Symmetric models (broken $SU(2)_L \times SU(2)_R$) or in GUT models which may also imply supersymmetry (e.g. E_6). Assuming the most general case, the new gauge group can comprise a new mixing angle ξ , new couplings to the fermions g' and a new CKM matrix U' . In some models the W' is right-handed and decays therefore into a right-handed neutrino and a lepton, however such a neutrino has not yet been observed. Because of this, the mass limits on the W' boson will depend on ξ , g' , U' and masses of additional neutrinos.

We make the assumption, that there is no mixing, g' equals the SM coupling, U' equals to the SM CKM matrix, and that new decay channels (like $W' \rightarrow WZ$) are suppressed. Furthermore, the width $\Gamma_{W'}$ of the W' boson is assumed to scale with its mass $m_{W'}$,

$$\Gamma_{W'} = \frac{4}{3} \cdot \frac{m_{W'}}{m_W} \cdot \Gamma_W. \quad (1)$$

The additional factor of 4/3 is applied in order to account for the decay into the third quark family (e.g. $W' \rightarrow t\bar{b}$), which is possible for $m_{W'}$ above 180 GeV. In case of the existence of additional generations of leptons, it is assumed that they are too heavy to be produced by a W' decay. Previous direct searches ($W' \rightarrow q\bar{q}'$, DØ, Run I) applying the constraints mentioned above exclude a W' boson with $m_{W'} < 800$ GeV at the 95% confidence level [2]. A complete review of direct (and indirect) searches for additional charged gauge bosons can be found in [3].

II. DATA AND BACKGROUND MONTE CARLO SAMPLES

Data collected with the DØ Detector at the Fermilab Tevatron collider at a center-of-mass energy of 1.96 TeV between August 2002 and February 2006 is used in this analysis. The dataset corresponds to an integrated luminosity of 900 pb⁻¹.

Different SM processes contribute to the (inclusive) electron + missing transverse energy final state: $W \rightarrow e\nu X$, $W \rightarrow \tau\nu X \rightarrow e\nu X$, $Z \rightarrow \tau\tau X \rightarrow e\nu X$, $WW \rightarrow e\nu X$, $ZZ \rightarrow ee\nu\nu$, $WZ \rightarrow e\nu X$ and $t\bar{t} \rightarrow e\nu X$. In these processes the missing energy is produced by the neutrino. There are also two sources of misidentification background that can contribute to this final state: QCD multijet background with one jet misidentified as an electron and energy mismeasurement which can cause large missing energy, and $Z \rightarrow ee$ events where one electron is lost (e.g. going into non-instrumented sections of the calorimeter) or misreconstructed. The latter case can contribute to large missing energies. The QCD multijet background is estimated from data.

The SM processes have been simulated with PYTHIA [4] using the CTEQ6L1 [5] parton distribution function (PDF). The events, which have been combined with zero bias events from data, were passed through the full detector simulation.

III. THE W' SIGNAL

Signal events for the channel $p\bar{p} \rightarrow W' + X \rightarrow e\nu + X$ have been generated with the Monte Carlo generator PYTHIA 6.323 [4] using the CTEQ6L1 [5] parton distribution function (PDF). These events have been combined with zero bias events from data and processed through the full detector simulation. Next-to-next-to leading order corrections to the PYTHIA leading order cross sections (K factors) have been applied. The K factors and errors due to PDF uncertainties are extracted from [6]. The NNLO cross sections and uncertainties are summarized in Tab. I.

From the numbers in the table one can see that the cross section falls steeply with increasing mass of the W' boson. Another effect of the heavier bosons is shown in the plot in Fig. 1: for very large masses the Jacobian distribution is blurred and no longer visible as a 'peak'; the distribution of the transverse mass is flat over a large range. Further studies have shown that the major part ($\approx 80\%$) of the electrons stemming from the W' decays are emitted into the central detector region, namely in the central calorimeter, which covers the range $-1.1 < \eta_{\text{det}} < 1.1$ ("CC"). Because of this, only the CC region has been studied.

FIG. 1: Transverse mass m_T distributions for different masses of the W' boson (generator level).

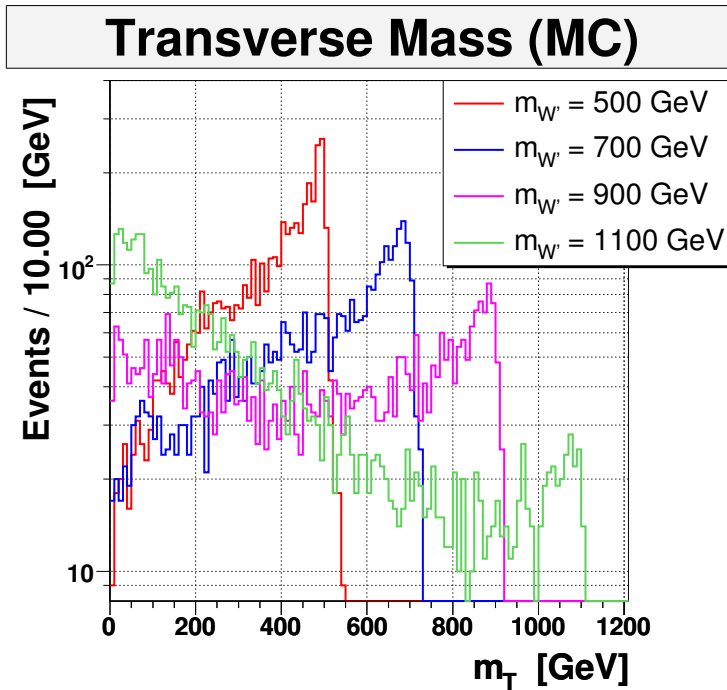


TABLE I: Cross sections and uncertainties due to PDF uncertainties for different masses of the W' boson.

$m_{W'}$ [GeV]	$\sigma_{W'} \times B(W' \rightarrow e\nu)$ [pb]		
	NNLO cross section	uncertainty (+)	uncertainty (-)
500	2.44	0.08	0.14
600	0.84	0.03	0.06
700	0.30	0.01	0.02
800	0.11	0.01	0.01
900	0.044	0.003	0.005
1000	0.019	0.001	0.002
1100	0.0095	0.0007	0.0012
1200	0.0056	0.0004	0.0007

IV. DATA SELECTION

Only triggered events are considered. The selected single electron triggers have the following generic trigger level requirements:

Level 1: energy deposit in the electromagnetic part of the calorimeter

Level 2: electromagnetic object with minimum transverse energy; there is no Level 2 constraint in some trigger lists

Level 3: tightening of the electromagnetic object (shower shape, electromagnetic fraction).

Electrons with transverse energy $E_T > 30$ GeV within $|\eta_{\text{det}}| < 1.1$ (central calorimeter) are required to pass the electron/photon identification criteria. Electromagnetic clusters are built around a calorimeter seed or around a track extrapolated into the calorimeter. Such clusters consist of cells in a cone ($\Delta R = \sqrt{(\Delta\eta)^2 + (\Delta\phi)^2} < 0.4$) around the seed. Electromagnetically interacting particles deposit most of their energy in the EM part of the calorimeter. Furthermore, the electron shower is required to be isolated. A requirement on the χ^2 value of the electron shower shape variable is applied to separate electromagnetic from hadronic showers. The electron is required to have a track

matched in z and ϕ direction and to stem from the primary vertex. The energy dependence of the basic electron reconstruction criteria has been studied with Monte Carlo electrons from W' decays. The reconstruction efficiency does not exhibit any energy dependence.

Jets are not part of the final state, but may be present in an event and contribute to missing energy. Jets are only looked at, if they pass standard jet identification criteria.

The raw missing transverse energy is calculated from all calorimeter cells. All corrections (electromagnetic and jet energy scale) are applied on the raw missing energy. Furthermore, the energy deposit of muons and their momentum are also taken into account. This fully corrected quantity (MET, \cancel{E}_T) is used in the analysis. We require $\cancel{E}_T > 30$ GeV.

Furthermore, the following requirements are applied:

- vertex constraints
 - primary vertex position $|z_{\text{vtx}}| < 60$ cm,
 - number of tracks associated to the vertex ≥ 3 ;
- ratio of electron energy and missing energy $0.7 < E_T / \cancel{E}_T < 1.3$;
- if jets with $E_T > 15$ GeV are present
 - $\Delta\phi(\text{jet}, \text{electron}) < 2.5$,
 - $\Delta\phi(\text{jet}, \text{MET}) < 2.5$.

The requirement on the ratio of the transverse energy of the electron and missing transverse energy is applied in order to select balanced events in terms of transverse energy. Jets – if present – are required *not* to be back-to-back to electron and missing energy in order to remove QCD di-jet events. In these events one jet is misidentified as an electron, together with energy mismeasurement, which results in large missing energy produced in the opposite direction of the jet.

The contribution from QCD di-jet events is estimated using a special sample derived from data. In this sample, the electron candidate fails the shower shape requirement. The resulting events are scaled to the data sample. The scale factor f_{QCD} is adjusted in the low reconstructed mass region ($m_T < 30$ GeV, dominated by QCD background events) to fill the missing events between the Monte Carlo prediction and observed data (left hand plot in Fig. 2). The transverse mass m_T is calculated from the transverse energy of the electron E_T , the missing transverse energy \cancel{E}_T and the azimuthal angle between the electron and the missing transverse energy via

$$m_T = \sqrt{2E_T \cancel{E}_T (1 - \cos \Delta\phi(\text{electron}, \text{MET}))} \quad (2)$$

The overall normalization is performed in the W peak region ($60 \text{ GeV} < m_T < 140 \text{ GeV}$, right hand plot in Fig. 2). Comparing data and Monte Carlo expectation in this region a luminosity of 900 pb^{-1} is derived.

V. RESULTS

A good agreement between data and Monte Carlo prediction can be observed. In Fig. 3 the following distributions are shown: electron transverse energy E_T , missing transverse energy MET , and the complete spectrum of the transverse mass m_T . The numbers corresponding to the plots are given in Tab. II, including a breakdown of the individual contributions of the different processes.

A. Systematic Uncertainties

Two kinds of systematical uncertainties contribute in this analysis: global normalization uncertainties (**NE**) and shape changing uncertainties (**SE**).

- **Cross section uncertainties (NE)**
The cross section uncertainties are of the magnitude of 4-10%.
- **Overall normalization (NE)**
The overall normalization uncertainty is estimated to 4%.

FIG. 2: After scaling the QCD sample (yellow) with f_{QCD} to the data, the agreement at low transverse masses (left hand plot) is good. The W peak region (right hand plot) is described by the sum of the SM Monte Carlo samples and the scaled QCD sample.

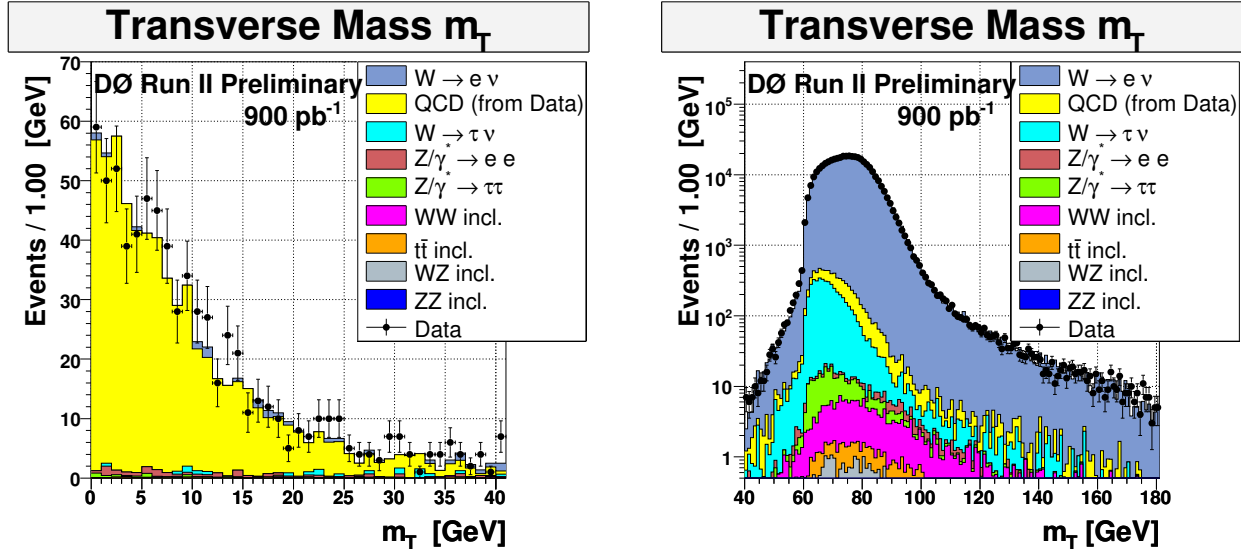


TABLE II: Remaining events in the data sample compared to the Monte Carlo prediction.

Process	Events	Statistical error	Systematical error	
			(+)	(-)
Data	396336			
Sum Backgrounds	395852.16	487.22	32344.16	36783.75
$W \rightarrow e\nu$	387455.10	482.23	31693.59	36122.51
$W \rightarrow \tau\nu$	4465.00	47.52	717.30	697.94
$Z \rightarrow ee$	80.69	3.96	8.45	10.36
$Z \rightarrow \tau\tau$	197.54	5.96	27.62	28.99
$WW, WZ, ZZ, t\bar{t}$ (incl.)	245.99	4.46	25.81	28.70
QCD (from data)	3407.83	50.07	136.31	136.31

- **Efficiency correction for electron reconstruction (NE)**

The uncertainty on the efficiency correction is $\sim 2\%$.

- **QCD scale factor f_{QCD} (NE)**

The uncertainty on the scale factor is estimated to 4%.

- **Electron energy scale and resolution (SE)**

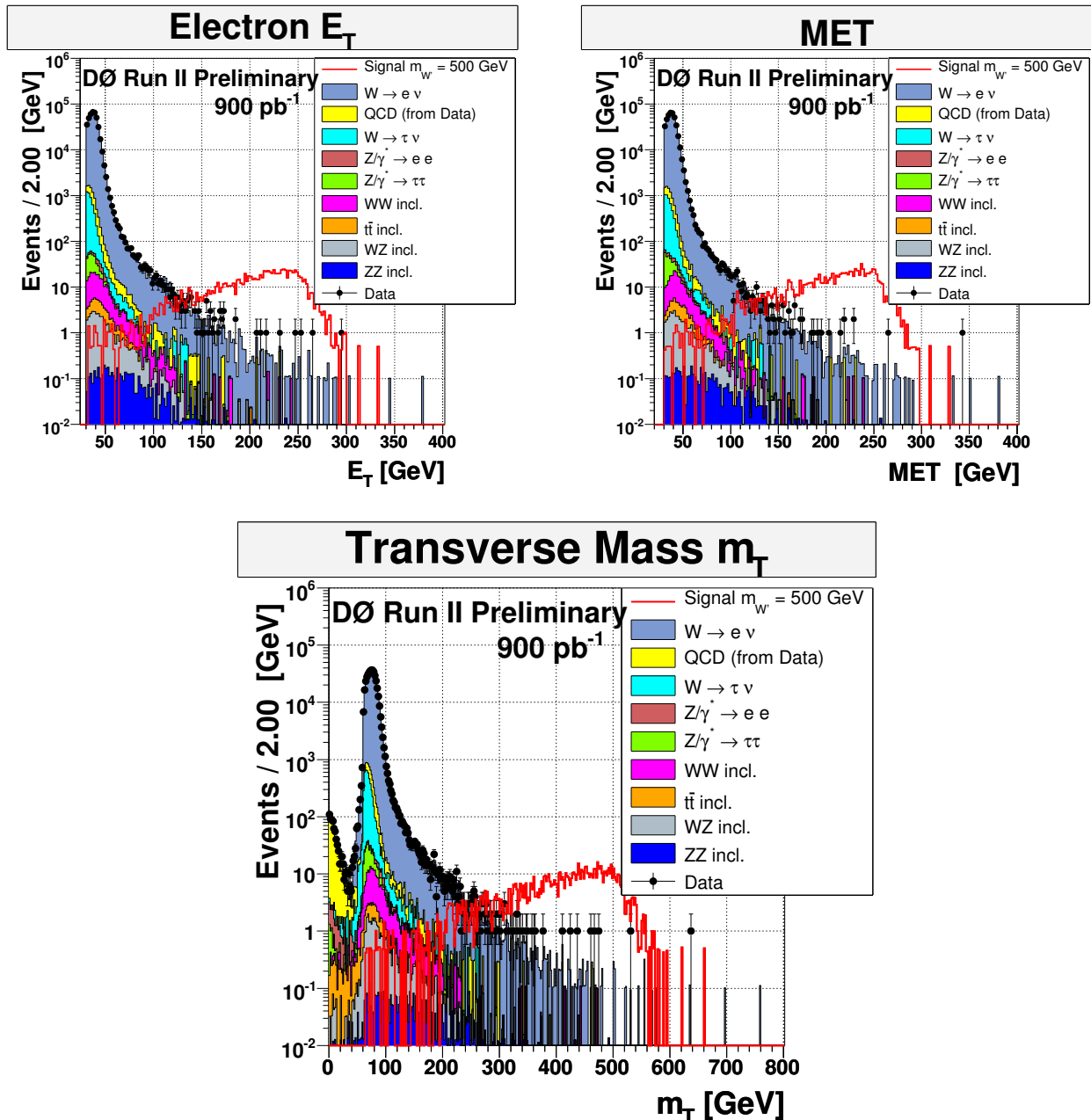
In order to study the effect of the electron energy scale and resolution, the electron energies E have been varied within the known uncertainties. The variation of scale and resolution are performed independently. The missing energy has been recalculated after varying the electron energy.

The overall uncertainty is large for the W sample (4% due to the requirement on the electron E_T in the steeply increasing region), but rather small for the signal ($< 1\%$). The uncertainty of the energy resolution is an order of magnitude smaller compared to the energy scale uncertainty.

- **PDF uncertainty (SE)**

In order to study the PDF uncertainty, the Monte Carlo events which have been produced using CTEQ6L1 are reweighted to CTEQ6.1M.xx (xx=0, ..., 40), making use of the CTEQ6.1M PDF and the 40 error functions ([7]). The overall uncertainty varies from 14% ($m_{W'} = 500$ GeV) to 45% ($m_{W'} = 1200$ GeV). For the W sample an uncertainty of 3% is derived.

FIG. 3: Comparison between data and Monte Carlo prediction. The following distributions are shown: electron transverse energy E_T , missing transverse energy MET and transverse mass m_T . The signal is plotted for a W' boson with $m_{W'} = 500$ GeV.



- **Uncertainty of the width Γ_W of the W (SE)**

The width of the W boson is known at the 2% level ([3]). In order to estimate this uncertainty, events are reweighted, so that there is no need for generating events with $\Gamma_W \pm \Delta\Gamma_W$. The weights are given by the Breit-Wigner ratio at the same mass. This effect causes a shift ($\sim 4\%$) of the tail of the transverse mass distribution of the W .

- **Jet energy scale (SE)**

The jet energy scale has been varied, and the missing energy recalculated. This effect has been taken into account, although it causes just a minor uncertainty of $\sim 1\%$.

TABLE III: Remaining events in the data sample compared to the Monte Carlo prediction after applying the requirement on the transverse mass $m_T > 150$ GeV.

Process	Events	Statistical error	Systematical error	
			(+)	(-)
Data	630			
Sum Backgrounds	622.93	17.91	82.65	75.25
$W \rightarrow e\nu$	572.73	17.49	77.42	71.19
$W \rightarrow \tau\nu$	10.10	2.26	3.37	1.86
$Z \rightarrow ee$	0.07	0.03	0.01	0.01
$Z \rightarrow \tau\tau$	1.11	0.08	0.32	0.18
$WW, WZ, ZZ, t\bar{t}$ (incl.)	15.47	1.08	2.57	2.75
QCD (from data)	23.46	2.97	0.94	0.94
$W' \rightarrow e\nu$ (500 GeV)	1032.16	22.45	164.19	164.00
$W' \rightarrow e\nu$ (600 GeV)	349.91	7.39	61.42	61.87
$W' \rightarrow e\nu$ (700 GeV)	131.02	2.93	30.92	29.93
$W' \rightarrow e\nu$ (800 GeV)	46.16	1.05	13.68	13.07
$W' \rightarrow e\nu$ (900 GeV)	16.64	0.39	6.86	6.06
$W' \rightarrow e\nu$ (1000 GeV)	6.56	0.16	3.54	2.95
$W' \rightarrow e\nu$ (1100 GeV)	3.01	0.07	1.76	1.36
$W' \rightarrow e\nu$ (1200 GeV)	1.51	0.04	0.78	0.58

B. Extraction of the Limit on the Production Cross Section

Since we do not see any significant excess in the data, an upper limit is set on the production cross section times branching ratio $\sigma_{W'} \times B(W' \rightarrow e\nu)$.

A Bayesian approach leads to upper limits on $\sigma_{W'} \times B(W' \rightarrow e\nu)$ for the several different resonance masses. A Poisson distribution is assumed for the number of expected events in each bin, as well as flat prior probabilities for the signal cross sections. The prior for the combined signal acceptance and background yields is a multivariate Gaussian with uncertainties and correlations described by a covariance matrix.

Since the regions of low and intermediate transverse masses have already been used for the scaling (QCD and overall normalization), the tail of the spectrum is now considered ($m_T > 150$ GeV). A good agreement between data and Monte Carlo prediction can be observed. In Tab. III a breakdown of the individual contributions of the various background processes is given, including expected numbers of signal events.

The limit is derived using a binned likelihood for the whole transverse mass spectrum $m_T > 150$ GeV. The individual shape changing systematics (up and down variation) enter the limit calculation via individual histograms; bin correlations are taken into account.

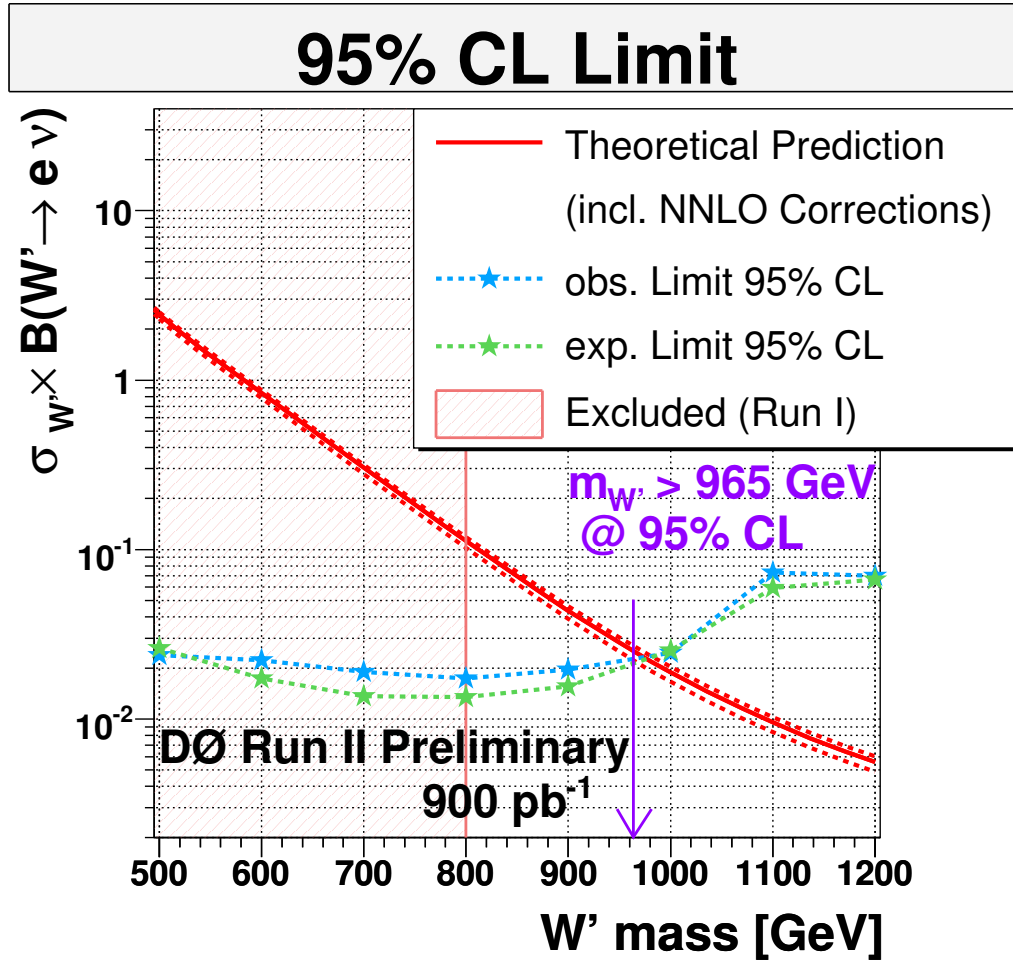
The 95% CL limit on the production cross section times branching ratio $\sigma_{W'} \times B(W' \rightarrow e\nu)$ is shown in Fig. 4. The red curve displays the theoretical expectation including the uncertainty (the NNLO cross sections are taken from Tab. I). Additional heavy charged gauge bosons with masses below 965 GeV can be excluded at the 95% CL, assuming that the new boson has the same couplings to fermions as the standard model W boson.

VI. SUMMARY

A search for additional heavy charged gauge bosons W' decaying in the electron channel has been performed for the first time at the $D\mathcal{O}$ experiment in Run II. Since we do not see a significant excess in data, an upper limit is set on the mass of an additional gauge boson, assuming that the new boson has the same couplings to fermions as the standard model W boson:

$$m_{W'} > 965 \text{ GeV} \quad @ \quad 95\% \text{ CL.} \quad (3)$$

FIG. 4: The 95% CL limit on the mass of the W' boson, including statistical and systematical errors. The red curve displays the theoretical expectation with uncertainty. The Run I limit is extracted from [2].



VII. ACKNOWLEDGMENTS

We thank the staffs at Fermilab and collaborating institutions, and acknowledge support from the DOE and NSF (USA); CEA and CNRS/IN2P3 (France); FASI, Rosatom and RFBR (Russia); CAPES, CNPq, FAPERJ, FAPESP and FUNDUNESP (Brazil); DAE and DST (India); Colciencias (Colombia); CONACyT (Mexico); KRF and KOSEF (Korea); CONICET and UBACyT (Argentina); FOM (The Netherlands); PPARC (United Kingdom); MSMT (Czech Republic); CRC Program, CFI, NSERC and WestGrid Project (Canada); BMBF and DFG (Germany); SFI (Ireland); Research Corporation, Alexander von Humboldt Foundation, and the Marie Curie Program.

-
- [1] R. N. Mohapatra, *Unification and Supersymmetry*, Springer (2003)
 - [2] DØ Collaboration, Phys. Rev. D **69**, 111101 (2004)
 - [3] Review of Particle Physics, S. Eidelman et al., Phys. Lett. B **592**, 1 (2004)
 - [4] T. Sjöstrand, Comp. Phys. Commun. **82** 74 (1994), CERN-TH 7112/93 (1993)
 - [5] J. Pumplin, D.R. Stump, J. Huston, H.L. Lai, P. Nadolsky, W.K. Tung, hep-ph/0201195
 - [6] R. Hamberg, W. L. van Neerven and T. Matsuura, Nucl. Phys. B **359**, 343 (1991); Erratum-ibid. B **644**, 403 (2002)
 - [7] J. Pumplin, D.R. Stump, J. Huston, H.L. Lai, W.K. Tung, S. Kuhlmann, J. Owens, hep-ph/0303013